Dissipation via Landau Damping in Two- and Three-Dimensional Plasma Turbulence

Tak Chu Li,[1] Gregory G. Howes,[1] Kristopher G. Klein,[2] and Jason M. TenBarge[3]

[1]*Department of Physics and Astronomy, University of Iowa, Iowa City, Iowa 52242, USA*
[2]*Space Science Center, University of New Hampshire, Durham, New Hampshire 03824, USA*
[3]*IREAP, University of Maryland, College Park, Maryland 20742, USA*

Plasma turbulence is ubiquitous in space and astrophysical plasmas, playing an important role in plasma energization, but the physical mechanisms that lead to dissipation of the turbulent energy remain to be definitively identified. This work addresses the fundamental physics of turbulent dissipation by examining the velocity-space structure that develops as a result of the collisionless interaction between the turbulent electromagnetic fluctuations and the particles in a low beta plasma. Both two- and three-dimensional (2D and 3D) nonlinear gyrokinetic simulations show an electron velocity-space signature qualitatively similar to that of the linear Landau damping of Alfvén waves in a 3D linear simulation. This evidence strongly suggests that the turbulent energy is transferred by Landau damping to electrons in low beta plasmas in both 2D and 3D, making possible the ultimate irreversible heating of the plasma. Although, in the 2D case with no variation along the equilibrium magnetic field, it may be expected that Landau damping is not possible, a common trigonometric correction factor appears in both the resonant denominator and the linear wave frequency, leading to an essentially unchanged resonance condition from the 3D case. Nonetheless, though the qualitative evolution of the 2D and 3D cases is similar, quantitatively the nonlinear energy transfer and subsequent dissipation is substantially slower in the 2D case.

arXiv:1510.02842v1 [astro-ph.SR] 9 Oct 2015

Introduction.—Plasma turbulence is ubiquitous in space and astrophysical plasmas, playing a governing role in the transfer of energy from large-scale motions down to small scales, where that energy is ultimately converted to plasma heat. A fundamental question at the frontier of astrophysics is what physical mechanisms determine the dissipation of the turbulence, specifically how the energy of the turbulent fluctuations in a weakly collisional plasma is ultimately converted to heat or other forms of particle energization.

To investigate numerically the dynamics of the collisionless wave-particle interactions that lead to damping of the turbulent electromagnetic fluctuations requires kinetic simulations, but their high-dimensionality requires significant computational power that often limits numerical studies to only two spatial dimensions (2D) [1–13]. How this limitation to 2D constrains the available energy dissipation pathways remains an open question [14–16].

In this Letter, we present gyrokinetic simulations showing the first evidence for Landau damping as the common pathway leading to turbulent dissipation in 2D and 3D nonlinear simulations, both leading to a velocity-space signature qualitatively similar to that of the linear Landau damping of Alfvén waves in a 3D linear simulation. Although, in the 2D case with no variation along the equilibrium magnetic field, it may be expected that Landau damping is not possible, we explain why the limitation to 2D does not prohibit Landau damping. This 2D limitation does, however, alter the quantitative evolution of the energy, likely due to a less rapid nonlinear cascade of energy to small scales compared to the 3D case.

Code.—The simulations presented here were performed using `AstroGK`, the Astrophysical Gyrokinetics Code. A detailed description of the code, including linear and nonlinear benchmarks, are presented in Ref. [17], so we give here only a brief overview.

`AstroGK` evolves the perturbed gyroaveraged distribution function $h_s(x, y, z, \lambda, \varepsilon)$ for each species s, the scalar potential φ, parallel vector potential $A_\parallel$, and the parallel magnetic field perturbation $\delta B_\parallel$ according to the gyrokinetic equation and the gyroaveraged Maxwell's equations [18, 19], where '$\parallel$' is along the total local magnetic field $\mathbf{B} = B_0\hat{\mathbf{z}} + \delta\mathbf{B}$. The velocity space coordinates are $\lambda = v_\perp^2/v^2$ and $\varepsilon = v^2/2$. The domain is a periodic box of size $L_\perp^2 \times L_z$, elongated along the equilibrium magnetic field, $\mathbf{B}_0 = B_0\hat{\mathbf{z}}$. Note that, in the gyrokinetic formalism, all quantities may be rescaled to any parallel dimension satisfying $L_z/L_\perp \gg 1$. Uniform Maxwellian equilibria for ions (protons) and electrons are used. Spatial dimensions (x, y) perpendicular to the equilibrium field are treated pseudospectrally; an upwind finite-difference scheme is used in the parallel direction. Collisions are incorporated using a fully conservative, linearized collision operator that includes energy diffusion and pitch-angle scattering [20, 21].

Diagnostics.—Two diagnostics are used to explore the energetics and velocity-space structure in the 2D and 3D turbulence simulations. The *energy diagnostic* examines the partitioning of energy among the terms of the fluctuating energy in the simulations. Consider a kinetic plasma with each species distribution function separated into an equilibrium and a fluctuating part, $f_s = F_{0s} + \delta f_s$. `AstroGK` evolves the perturbed distribution function, δf_s, making it possible to follow the exchange of energy within the *total fluctuating energy* [19, 22, 23] given by

$$\delta W = \int d^3\mathbf{r} \left[\frac{|\delta\mathbf{B}|^2 + |\delta\mathbf{E}|^2}{8\pi} + \sum_s \left(\frac{1}{2} n_{0s} m_s |\delta\mathbf{u_s}|^2 + \frac{3}{2}\delta P_s \right) \right]. \quad (1)$$

Note that this fluctuating energy includes neither the equilibrium thermal energy, $\int d^3\mathbf{r} \int d^3\mathbf{v} \frac{1}{2} m v^2 F_{0s} = \frac{3}{2} n_s T_{0s}$, nor the equilibrium magnetic field energy, $\int d^3\mathbf{r}\ B_0^2/8\pi$. Thus, the terms of δW represent the perturbed electromagnetic field energies and the species bulk kinetic and non-thermal energies.

The *turbulent energy* is defined as the sum of the electromagnetic field and the bulk kinetic energies [24], $E^{(turb)} \equiv \int d^3\mathbf{r}[(|\delta\mathbf{B}|^2 + |\delta\mathbf{E}|^2)/8\pi + \sum_s \frac{1}{2} n_{0s} m_s |\delta\mathbf{u_s}|^2]$. This sum comprises the turbulent energy because the linear terms in the evolution equations (primarily the effect of magnetic tension) lead to an oscillatory sloshing of energy between magnetic and bulk kinetic energies. The *non-thermal energy* in the distribution function (minus bulk flows) is defined by $E_s^{(nt)} \equiv \int d^3\mathbf{r} \frac{3}{2} \delta P_s \equiv \int d^3\mathbf{r} (\int d^3\mathbf{v}\ T_{0s} \delta f_s^2 / 2F_{0s} - \frac{1}{2} n_{0s} m_s |\delta\mathbf{u_s}|^2)$ [25].

The flow of energy in our kinetic turbulence simulations follows a simple path. As the system evolves, first, nonlinear interactions transfer the turbulent energy from large to small spatial scales. Then, when the energy has reached sufficiently small spatial scales, collisionless wave-particle interactions transfer energy from the electromagnetic fields to non-thermal energy in the particle distributions. This non-thermal energy in δf_s manifests as small-scale structures in the velocity space, which are ultimately smoothed out by collisions, irreversibly converting the non-thermal energy into thermal energy, and thereby increasing the entropy of the plasma [19]. In `AstroGK`, the effect of collisions is to remove energy from δW. The collisional energy loss from δW, denoted $E_s^{(coll)}$, is tracked by the energy diagnostic, representing thermal heating of the species, but this energy is not fed back into the equilibrium thermal temperature, T_{0s} [17, 19].

The *velocity-space diagnostic* probes structures in velocity space that arise from the collisionless damping of the turbulent fluctuations. To first-order in gyrokinetic theory [19], the distribution function is given by

$$f_s(v_\parallel, v_\perp) = \left(1 - \frac{q_s \varphi}{T_{0s}}\right) F_{0s}(v) + h_s(v_\parallel, v_\perp), \quad (2)$$

where $F_{0s} = (n_{0s}/\pi^{3/2} v_{ts}^3) \exp(-v^2/v_{ts}^2)$ is the equilibrium Maxwellian distribution, $q_s\varphi/T_{0s}$ is the Boltzmann term, h_s is the first-order gyroaveraged part of the perturbed distribution. Explicit spatial dependence is repressed for simplicity. The study of Alfvénic fluctuations and their collisionless damping is made clearer by examining the complementary distribution function [23],

$$g_s(v_\parallel, v_\perp) = h_s(v_\parallel, v_\perp) - \frac{q_s F_{0s}}{T_{0s}} \left\langle \varphi - \frac{\mathbf{v}_\perp \cdot \mathbf{A}_\perp}{c} \right\rangle_{\mathbf{R}_s}, \quad (3)$$

where $\langle ... \rangle$ represents a gyrophase angle average at constant guiding center $\mathbf{R}_s$. By plotting $g_s(v_\parallel, v_\perp) \exp(+v^2/v_{ts}^2)$, we eliminate the exponential energy dependence of g_s, highlighting non-Maxwellian structures that arise through collisionless damping of the turbulent fluctuations.

Simulations.—The 2D Orszag-Tang Vortex (OTV) problem [26], and various 3D generalizations, have been widely used to study plasma turbulence [2, 13, 27–32]. We specify here a particular 3D formulation of the initial conditions (denoted $OTV3D$), given in Elsässer variables, $\mathbf{z}^\pm \equiv \delta\mathbf{u} \pm \delta\mathbf{B}/\sqrt{4\pi\rho_0}$, by

$$\begin{aligned} \frac{\mathbf{z}_1^+}{v_A} &= -\frac{2z_0}{v_A}\,\hat{\mathbf{x}}\,\sin(k_\perp y - k_\parallel z), \quad \frac{\mathbf{z}_1^-}{v_A} = 0 \\ \frac{\mathbf{z}_2^\pm}{v_A} &= \frac{z_0}{v_A}\,\hat{\mathbf{y}}\,\sin(k_\perp x \mp k_\parallel z) \\ \frac{\mathbf{z}_3^\pm}{v_A} &= \pm\frac{z_0}{v_A}\,\hat{\mathbf{y}}\,\sin(2k_\perp x \mp k_\parallel z) \end{aligned} \quad (4)$$

where $v_A = B_0/\sqrt{4\pi\rho_0}$ is the Alfvén speed, $\rho_0 = m_i n_0$ is the mass density, $\delta\mathbf{u}$ and $\delta\mathbf{B}$ are perturbations in the proton bulk velocity and the magnetic field, and $k_\perp$ and $k_\parallel$ are positive constants. This 3D generalization consists of counterpropagating Alfvén waves along $B_0\hat{\mathbf{z}}$. On the mid-plane ($z = 0$), the 3D formulation reduces to the familiar 2D OTV setup ($OTV2D$), given by

$$\begin{aligned} \delta\mathbf{u} &= \delta u[-\sin(k_\perp y)\hat{\mathbf{x}} + \sin(k_\perp x)\hat{\mathbf{y}}] \\ \delta\mathbf{B} &= \delta B[-\sin(k_\perp y)\hat{\mathbf{x}} + \sin(2k_\perp x)\hat{\mathbf{y}}], \end{aligned} \quad (5)$$

where $z_0 = \delta u = \delta B/\sqrt{4\pi\rho_0}$.

To resolve the kinetic mechanisms mediating the conversion of turbulent energy to plasma energy, including Landau damping and collisionless magnetic reconnection, it is necessary to follow the turbulent cascade from the inertial range at $k_\perp \rho_i \ll 1$ to below the electron scales, $k_\perp \rho_e > 1$ [25, 33, 34]. Therefore, we specify an artificially reduced mass ratio, $m_i/m_e = 25$, so that with a simulation domain size of $L_\perp = 8\pi\rho_i$ and simulation dimensions $(n_x, n_y, n_z, n_\lambda, n_\varepsilon, n_s) = (128, 128, 32, 64, 32, 2)$ in 3D (with $n_z = 2$ in 2D), we resolve a dynamic range of scales of $0.25 \le k_\perp\rho_i \le 10.5$, or $0.05 \le k_\perp\rho_e \le 2.1$.

Plasma parameters are ion plasma beta $\beta_i = 8\pi n_i T_i/B_0^2 = 0.01$ and $T_i/T_e = 1$. Under $\beta_i \ll 1$ conditions, the ion dynamics are expected to contribute negligibly to the collisionless damping via the Landau resonance. Collision frequencies of $\nu_i = 10^{-5}\omega_{A0}$ and $\nu_e = 0.05\ \omega_{A0}$ (where $\omega_{A0} \equiv k_\parallel v_A$ is a characteristic Alfvén wave frequency propagating along $\hat{\mathbf{z}}$ in 3D) are sufficient to keep velocity space well resolved [35, 36] and enable irreversible heating of the plasma species [19]. To obtain strong turbulence, we choose an initial amplitude that yields a nonlinearity parameter $\chi = k_\perp z_0/(k_\parallel v_A) = 1$, thereby achieving a state of critical balance [37] in the 3D run; the same amplitude z_0 is used in the 2D run. Time is normalized by the domain turnaround time $\tau_0 = L_\perp/z_0$ and velocity by the species thermal speed $v_{ts} = \sqrt{2T_s/m_s}$.

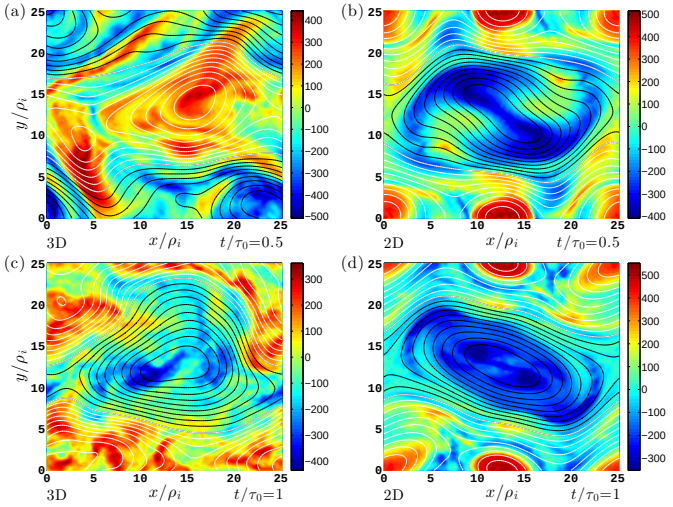

FIG. 1: Spatial profile of J_z (color) and $A_\parallel$ (contours) on the $z = 0$ plane of the OTV3D (left) and OTV2D (right) simulations at $t/\tau_0 = 0.5$ (top) and $t/\tau_0 = 1$ (bottom). Contours represent positive (white) and negative (black) values of $A_\parallel$.

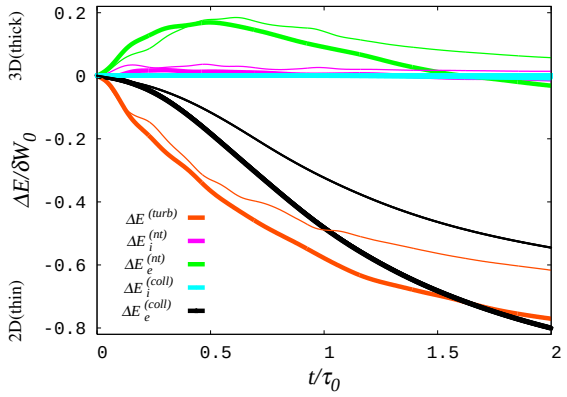

FIG. 2: Change of energy over total initial fluctuating energy, $\Delta E/\delta W_0$, for the turbulent energy $E^{(turb)}$ (orange), the non-thermal energy $E_s^{(nt)}$ of ions (magenta) and electrons (green), the collisionally dissipated energy $E_s^{(coll)}$ for ions (cyan) and electrons (black). Line thickness indicates OTV3D (thick) or OTV2D (thin) simulations.

Note that, for the reduced mass ratio, the low beta conditions satisfy $\beta_i < m_e/m_i$, so the Alfvén wave transitions to an inertial Alfvén wave [38] at small scales. In 3D, the initial counterpropagating Alfvén waves at the perpendicular domain scale $L_\perp$ have a frequency of $\omega = 0.93\omega_{A0}$, and the frequency drops slowly as the perpendicular scale decreases. Simulations with β_i=0.1, in which the Alfvén wave transitions instead to a kinetic Alfvén wave at small scales, show results similar to those presented here, so we believe the physical mechanism reported here is robust for low-β plasmas.

Evolution of the OTV.—The OTV setup consists of an initial flow and current pattern, which breaks up into turbulence before $t = \tau_0$. We plot in Fig. 1 the spatial profile of J_z (color) and $A_\parallel$ (contours) from the OTV2D and the $z = 0$ plane of the OTV3D simulations. At $t = 0.5\tau_0$, the initial double vortices near the center have merged completely in both cases, and thin current sheets have developed. Note that $t = 0.5\tau_0$ is roughly half of the Alfvén wave period, so the J_z pattern at $z = 0$ in 3D appears π *out of phase* (opposite colors) relative to the 2D case. At $t = \tau_0$, J_z in 3D returns to a configuration similar to the 2D case: negative (blue) current in the center surrounded by positive (red) currents. The nonlinear cascade of energy to small scales is more rapid in the 3D case, showing more energy in small-scale magnetic structures in Fig. 1; this is supported by comparing the magnetic energy spectra (not shown).

Evolution of Energy.—Next we consider the physical processes by which energy is removed from the turbulent fluctuations and ultimately converted to plasma heat.

It is worthwhile mentioning the dominant components of the turbulent energy in our simulations. For low-frequency electromagnetic waves, $|\delta\mathbf{E}|^2/|\delta\mathbf{B}|^2 \sim \mathcal{O}(v_A^2/c^2)$, so the electric field energy is negligible in the non-relativistic limit [19, 39]. Throughout the evolution, the turbulent energy $E^{(turb)}$ is dominated by the perpendicular magnetic and perpendicular ion bulk kinetic energy (more than 75%). The parallel electron bulk kinetic energy, supporting the currents in the simulation, contributes less than 20% of the energy, but this is artificially large due to the small mass ratio chosen, $m_i/m_e = 25$; for a realistic mass ratio of 1836, it is not expected to contribute significantly to the energy budget. Finally, the parallel magnetic, parallel ion bulk kinetic, and perpendicular electron bulk kinetic energies contribute less than 7% of the turbulent energy.

Fig. 2 shows the change in energy ΔE, relative to the initial total fluctuating energy δW_0, for the turbulent $E^{(turb)}$ (orange), non-thermal $E_s^{(nt)}$ (magenta, green), and collisionally dissipated $E_s^{(coll)}$ (cyan, black) energies, where line thickness indicates OTV3D (thick) or OTV2D (thin) simulations. Initially, turbulent energy (orange) is dominantly transferred into electron non-thermal energy (green). Physically, this occurs through a two-step process: (1) the turbulent energy is transferred nonlinearly to small spatial scales; and (2) at these small scales, collisionless wave-particle interactions transfer energy from the electromagnetic fields to the electrons as non-thermal energy in the velocity distribution, $E_e^{(nt)}$. At $t > 0.25\tau_0$,

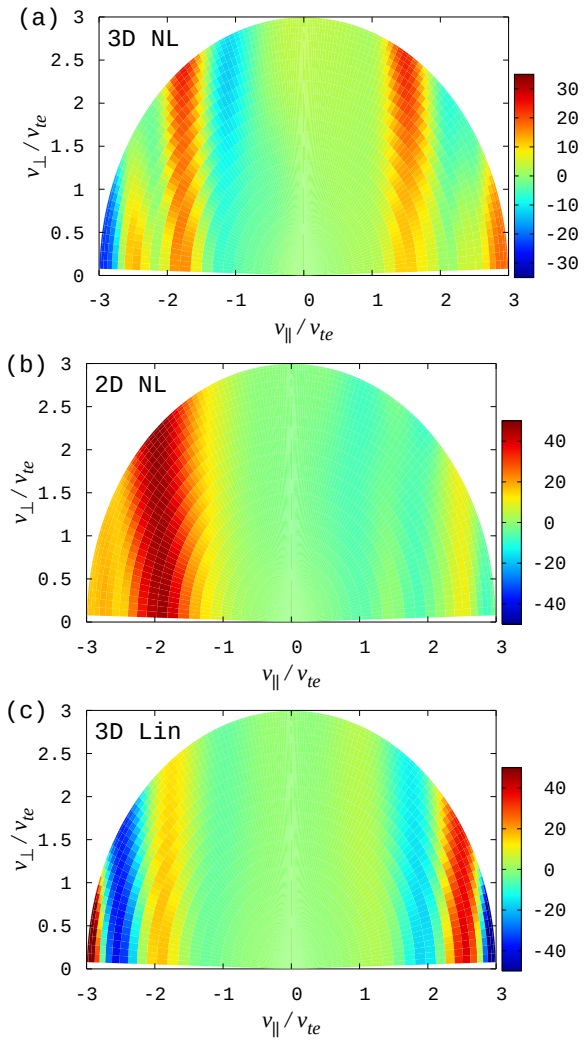

FIG. 3: Kinetic signature of Landau damping in the perturbed electron distribution, $\mathrm{Re}[g_e \exp(v^2/v_{te}^2)]$, for the (a) OTV3D and (b) OTV2D simulations, and for (c) a linear 3D simulation of the Landau damping of counterpropagating Alfvén waves.

the electron non-thermal energy begins to be significantly collisionally dissipated (black), indicating the ultimate thermalization of electron energy (which `AstroGK` removes from δW). As expected, ions play a negligible role in the dissipation of the turbulent energy at $\beta_i \ll 1$.

The qualitative evolution of the 2D case is remarkably similar to the 3D case, suggesting that the same kinetic physical mechanisms mediate the dissipation in both cases. Despite this qualitative similarity, quantitatively, the dissipation rate is significantly faster in 3D. By $t = 2\tau_0$, the 3D simulation has dissipated 80% of δW_0, but the 2D simulation has dissipated only 55%.

Landau damping.—To illuminate the physical mechanisms governing the dissipation of kinetic turbulence, we examine the electron velocity distribution in both 2D and 3D cases. In Fig. 3, we plot the velocity-space structure in the $z = 0$ plane, $\mathrm{Re}[g_e \exp(v^2/v_{te}^2)]$, for both (a) OTV3D and (b) OTV2D simulations for the wavevector mode $(k_x\rho_i, k_y\rho_i) = (1, 1)$ at the peak of the electron collisional dissipation rate at $t/\tau_0 \simeq 0.7$. This mode receives energy strictly via the turbulent nonlinear interactions that transfer energy from larger scale initial modes.

Fig. 3 shows that the kinetic signature in velocity space for both 2D and 3D simulations is qualitatively similar, with the development of structure strictly along $v_\parallel$ (essentially no variation along $v_\perp$). Collisionless wave-particle interactions via the Landau resonance with electrons are predicted to generate only $v_\parallel$ structure, and the Landau resonant velocity for this mode, $v_\parallel \simeq 1.4 v_{te}$, is consistent with the location of the structure in both 2D and 3D cases. An alternative way to describe Landau damping is *parallel phase mixing*, which leads to the damping of the electromagnetic fields through *mixing* of electron populations in parallel velocity space.

To confirm Landau damping as the dominant mechanism diminishing the turbulent energy $E^{(turb)}$, we plot in Fig. 3 (c) the velocity-space structure for a linear 3D simulation of two counterpropagating Alfvén waves of the same $(1, 1)$ mode as they Landau damp at the rate predicted by linear kinetic theory. A quantitative comparison of the linear to the nonlinear simulations is not meaningful, because the linear case models the decay of two initial Alfvén waves, whereas the nonlinear cases involve the continual nonlinear transfer of energy into the $(1, 1)$ mode. Nonetheless, the striking qualitative similarity between the linear Landau damping of Alfvén waves and the 2D and 3D nonlinear simulations provides strong new evidence that Landau damping is the dominant physical mechanism responsible for the damping of turbulent fluctuations, facilitating the subsequent collisional dissipation of the non-thermal energy. Furthermore, the velocity-space structure in the nonlinear simulations appears very similar to that of *linear* Landau damping, suggesting the kinetic dissipation is largely linear in nature, supporting a recent theoretical prediction [24].

In addition, a current sheet develops during the merging of the initial double vortices, and multiple thin current sheets arise later in both the 2D and 3D simulations (Fig. 1). Despite the development and dissipation of these coherent structures, the damping appears to be entirely consistent with Landau damping, supporting speculation that Landau damping dominates dissipation of current sheets in collisionless 3D kinetic Alfvén wave turbulence [33], and consistent with evidence of Landau damping in 2D simulations of magnetic reconnection [40].

Landau Damping in 2D?—For a 2D simulation with no variation along the equilibrium magnetic field $\mathbf{B}_0 = B_0\hat{\mathbf{z}}$, one may naively expect that Landau damping is prohibited. However, when there is an in-plane component such that the total field is $\mathbf{B} = B_0\hat{\mathbf{z}} + \delta B_\perp \hat{\mathbf{x}}$, the resonant

denominator responsible for Landau damping becomes $\omega - k_x v_\parallel \sin\theta$, where $\sin\theta = \delta B_\perp / |\mathbf{B}|$. The frequency of linear Alfvén waves propagating on the 2D plane is also modified to become $\omega = k_x v_A \sin\theta$. The trigonometric correction factors out, leaving a 2D resonant condition $v_\parallel \sim v_A$ that is essentially unchanged from the 3D case. This explains how Landau damping can be the dominant pathway to dissipation in both 2D and 3D kinetic turbulence simulations.

Conclusions.—By examining the kinetic signature of collisionless damping in the electron velocity distribution, we find evidence that Landau damping is the dominant mechanism converting turbulent energy to non-thermal electron energy in 2D and 3D nonlinear kinetic simulations of plasma turbulence at $\beta_i \ll 1$. The remarkable similarity in the velocity-space signature between the linear Landau damping of Alfvén waves and both the 2D and 3D nonlinear simulations suggests that this kinetic damping mechanism is essentially linear in nature [24]. In addition, although the qualitative evolution of the 2D and 3D cases is similar, quantitatively the nonlinear energy transfer and subsequent dissipation is substantially slower in the 2D case. Despite naive expectations that Landau damping is ineffective in 2D, the action of Landau damping in 2D simulations is explained theoretically by a common trigonometric correction factor appearing in both the resonant denominator and the linear wave frequency, leading to an essentially unchanged resonance condition. These results agree with previous findings that Landau damping is the dominant dissipation mechanism in plasma turbulence, even when current sheets develop and dissipate, as observed in 3D simulations of kinetic Alfvén wave turbulence [33, 34] and 2D simulations of strong-guide-field magnetic reconnection [40].

Supported by NSF CAREER Award AGS-1054061, NASA grant NNX10AC91G, and NSF grant AGS-1331355.

[1] S. P. Gary, S. Saito, and H. Li, Geophys. Res. Lett. **35**, 2104 (2008).

[2] T. N. Parashar, M. A. Shay, P. A. Cassak, and W. H. Matthaeus, Phys. Plasmas **16**, 032310 (2009).

[3] S. Servidio, F. Valentini, F. Califano, and P. Veltri, Phys. Rev. Lett. **108**, 045001 (2012).

[4] D. Verscharen, E. Marsch, U. Motschmann, and J. Müller, Phys. Plasmas **19**, 022305 (2012), arXiv:1201.2784 [physics.space-ph].

[5] M. Wan, W. H. Matthaeus, H. Karimabadi, V. Roytershteyn, M. Shay, P. Wu, W. Daughton, B. Loring, and S. C. Chapman, Phys. Rev. Lett. **109**, 195001 (2012).

[6] S. A. Markovskii and B. J. Vasquez, Astrophys. J. **768**, 62 (2013).

[7] D. Perrone, F. Valentini, S. Servidio, S. Dalena, and P. Veltri, Astrophys. J. **762**, 99 (2013), arXiv:1207.5379 [physics.space-ph].

[8] P. Wu, S. Perri, K. Osman, M. Wan, W. H. Matthaeus, M. A. Shay, M. L. Goldstein, H. Karimabadi, and S. Chapman, Astrophys. J. Lett. **763**, L30 (2013).

[9] P. Wu, M. Wan, W. H. Matthaeus, M. A. Shay, and M. Swisdak, Phys. Rev. Lett. **111**, 121105 (2013), arXiv:1306.4372 [physics.plasm-ph].

[10] H. Che, M. L. Goldstein, and A. F. Viñas, Phys. Rev. Lett. **112**, 061101 (2014), arXiv:1307.2615 [astro-ph.SR].

[11] C. T. Haynes, D. Burgess, and E. Camporeale, Astrophys. J. **783**, 38 (2014), arXiv:1304.1444 [physics.space-ph].

[12] Y. Narita, H. Comisel, and U. Motschmann, Frontiers in Phys. **2**, 13 (2014).

[13] T. N. Parashar, B. J. Vasquez, and S. A. Markovskii, Physics of Plasmas **21**, 022301 (2014).

[14] G. G. Howes, Journal of Plasma Physics **81**, 3203 (2015).

[15] M. Wan, W. H. Matthaeus, V. Roytershteyn, H. Karimabadi, T. Parashar, P. Wu, and M. Shay, Phys. Rev. Lett. **114**, 175002 (2015).

[16] S. Servidio, F. Valentini, D. Perrone, A. Greco, F. Califano, W. H. Matthaeus, and P. Veltri, Journal of Plasma Physics **81** (2015), 10.1017/S0022377814000841.

[17] R. Numata, G. G. Howes, T. Tatsuno, M. Barnes, and W. Dorland, J. Comp. Phys. **229**, 9347 (2010), arXiv:1004.0279 [physics.plasm-ph].

[18] E. A. Frieman and L. Chen, Phys. Fluids **25**, 502 (1982).

[19] G. G. Howes, S. C. Cowley, W. Dorland, G. W. Hammett, E. Quataert, and A. A. Schekochihin, Astrophys. J. **651**, 590 (2006), astro-ph/0511812.

[20] I. G. Abel, M. Barnes, S. C. Cowley, W. Dorland, and A. A. Schekochihin, Phys. Plasmas **15**, 122509 (2008), arXiv:0808.1300.

[21] M. Barnes, I. G. Abel, W. Dorland, D. R. Ernst, G. W. Hammett, P. Ricci, B. N. Rogers, A. A. Schekochihin, and T. Tatsuno, Phys. Plasmas **16**, 072107 (2009).

[22] A. J. Brizard and T. S. Hahm, Rev. Mod. Phys. **79**, 421 (2007).

[23] A. A. Schekochihin, S. C. Cowley, W. Dorland, G. W. Hammett, G. G. Howes, E. Quataert, and T. Tatsuno, Astrophys. J. Supp. **182**, 310 (2009).

[24] G. G. Howes, Philosophical Transactions of the Royal Society of London A: Mathematical, Physical and Engineering Sciences **373**, 20140145 (2015).

[25] J. M. TenBarge, W. Daughton, H. Karimabadi, G. G. Howes, and W. Dorland, Phys. Plasmas **21**, 020708 (2014).

[26] S. A. Orszag and C.-M. Tang, J. Fluid Mech. **90**, 129 (1979).

[27] H. Politano, A. Pouquet, and P. L. Sulem, Phys. Fluids B **1**, 2330 (1989).

[28] R. B. Dahlburg and J. M. Picone, Phys. Fluids B **1**, 2153 (1989).

[29] J. M. Picone and R. B. Dahlburg, Phys. Fluids B **3**, 29 (1991).

[30] H. Politano, A. Pouquet, and P. L. Sulem, Physics of Plasmas **2**, 2931 (1995).

[31] R. Grauer and C. Marliani, Phys. Rev. Lett. **84**, 4850 (2000).

[32] P. D. Mininni, A. G. Pouquet, and D. C. Montgomery, Phys. Rev. Lett. **97**, 244503 (2006), physics/0607269.

[33] J. M. TenBarge and G. G. Howes, Astrophys. J. Lett. **771**, L27 (2013), arXiv:1304.2958 [physics.plasm-ph].

[34] J. M. TenBarge, G. G. Howes, and W. Dorland, Astro-

phys. J. **774**, 139 (2013).
[35] G. G. Howes, W. Dorland, S. C. Cowley, G. W. Hammett, E. Quataert, A. A. Schekochihin, and T. Tatsuno, Phys. Rev. Lett. **100**, 065004 (2008).
[36] G. G. Howes, J. M. TenBarge, W. Dorland, E. Quataert, A. A. Schekochihin, R. Numata, and T. Tatsuno, Phys. Rev. Lett. **107**, 035004 (2011).
[37] P. Goldreich and S. Sridhar, Astrophys. J. **438**, 763 (1995).
[38] B. J. Thompson and R. L. Lysak, J. Geophys. Res. **101**, 5359 (1996).
[39] G. G. Howes, K. G. Klein, and J. M. TenBarge, Astrophys. J. **789**, 106 (2014), arXiv:1405.5460 [astro-ph.SR].
[40] R. Numata, N. F. Loureiro, and Loureiro, Journal of Plasma Physics **81**, 3001 (2015), arXiv:1406.6456 [physics.plasm-ph].